Supplementary On-Line Material for:

Unusually low thermal conductivity of atomically thin 2D tellurium

Zhibin Gao, Fang Tao, and Jie Ren*

Center for Phononics and Thermal Energy Science, China-EU Joint Center for Nanophononics, Shanghai Key Laboratory of Special Artificial Microstructure Materials and Technology, School of Physics Sciences and Engineering, Tongji University, Shanghai 200092, China

E-mail: Xonics@tongji.edu.cn

I. Crystal structure of β-tellurene

The crystal structure information of β-tellurene at PBE level in this letter is listed here: $a_1 = 5.731$, $a_2 = 4.219$ and $a_3 = 30.145$. There are three atoms in the unit cell. Atomic fractional coordinates are (0,0,0.5), (0.336,0.5,0.534) and (0.663,0.5,0.466), respectively.

II. Thermal conductivity T^{-1} behavior in tellurene

Generally speaking, there are two kinds of scattering processes that will affect the phonon relaxation time. One is N-type process and the other one is U-type process. Since G=0 (G is a reciprocal lattice vector), there is no thermal resistance in N-type process. However, U-type process will generate thermal resistance and nonlinear strength is usually proportional to the temperature. The thermal conductivity T^{-1} behaviour in bulk Te has been reported.[1] Here, our aim is to explore whether thermal conductivity in tellurene has a similar behavior.

After fitting, the results along x and y directions are κ_L = 652.3/T and κ_L = 1231.4/T, respectively. This nice $\kappa_L \propto T^{-1}$ behavior indicates a dominant phonon scattering by Umklapp process in 2D tellurene.

III. Correction of phonon dispersion

The phonon frequencies can be obtained from the eigenvalues of the dynamical matrix. Imaginary frequencies appear when the material is dynamically unstable through the imaginary phonon modes. Different from three linear acoustic phonon modes in 3D, there is an unique and interesting out-of-plane (ZA) mode in 2D materials. However, in order to get a converged ZA mode, one needs a very large supercell and dense k meshes, avoiding the artificial imaginary frequencies around the Γ point. Furthermore, in the long wavelength limit, ZA mode is quadratic in wave vector $\mathbf{q}$. Yet many times DFT gives a non-parabolic phonon modes. To bypass this issue, hence, we correct our ZA mode of tellurene based on the continuum approach for long-wavelength acoustic phonons.[4] The flexural rigidity D in 2D materials can be expressed as[4]

$$D = \frac{1}{2}\epsilon_b d^2 \tag{1}$$

in which ϵ_b and d are the bending energy divided by the surface area and the diameter of the tube made by 2D materials. The results are shown in Fig. S2. We can find that along the Γ-X direction, there is an obvious deviation between DFT calculation and continuum approach in 2D tellurene. Heat is mainly carried by the low frequency acoustic phonons and it has has been proved that this

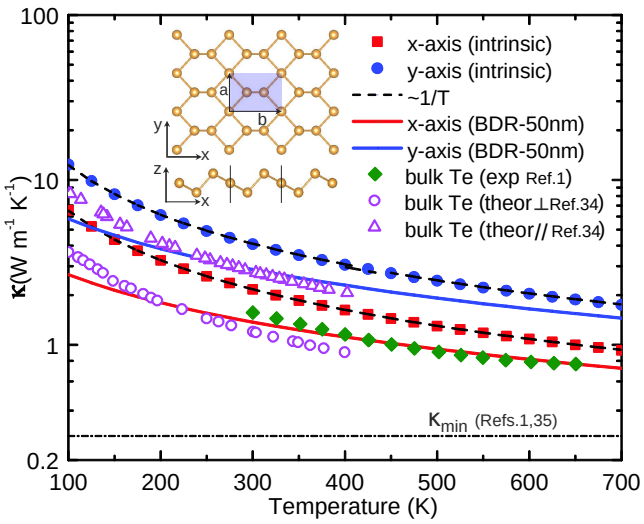

Fig. S1: Lattice thermal conductivity of tellurene as a function of temperature. Ball and stick model of the tellurene in top and side views are shown in the inset. The primitive cell is indicated by the blue shading in the top view. $\boldsymbol{a}$ and $\boldsymbol{b}$ are the lattice vectors spanning the 2D lattice. Black dashed lines are $1/T$ fitting of temperature dependent κ_L. The experimental data[1] of bulk Te are collected in green rhombic dots. The theoretical results[2] are gathered in purple triangles/circles along parallel/perpendicular to the bulk helical chains. The dashed lines are provided as a guide to the eye. Red cubics and blue dots are the intrinsic κ_L only with phonon-phonon scattering. Red and blue solid lines are the κ_L considering boundary scattering with a characteristic size of 50 nm according to Eq. (2). The dash dotted line is the lower limit κ_{min} of bulk Te from the previous experiment[1] that is based on the Cahill model.[3]

deviation will significantly lead to an overestimate κ_L.[5]

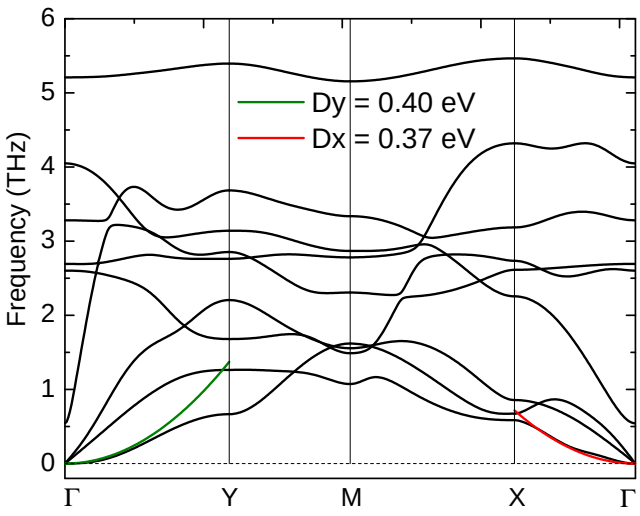

Fig. S2: Phonon spectra of tellurene shown by the black solid lines. The correction of flexural acoustic ZA mode based on the continuum approach is superposed in red and green solid lines along the x and y directions.

IV. Three-phonon scattering phase space in tellurene

In the three-phonon scattering process, all phonon modes must be satisfied the conservation of energy and momentum simultaneously. To measure the probability of three-phonon scattering, we use the phase space[12,13] to quantitatively show all available three-phonon scattering process in tellurene. The result is shown in Fig. S3. The larger phase space P_3 of three-phonon scattering channels is , the strong anharmonicity of the material has. In this sense, tellurene has more scattering channels compared with the bulk SnSe, indicating a strong anharmonicity in tellurene.

V. Length-dependent thermal conductivity in tellurene

We calculated the frequency-resolved κ_L and accumulated κ_L for tellurene. Similar to graphene and other 2D materials, in tellurene low frequency phonons dominate the contribution of κ_L in both x

Table S1: Relevant mechanical and thermal properties of phosphorene, 2D SnSe and tellurene. Sound velocities of TA phonon mode along x and y directions (υ^x_{TA} and υ^y_{TA}) in km/s; In-plane Young's modulus (E_x and E_y) in GPa; Shear modulus (G) in GPa; In-plane Poisson's ratio along x and y directions (ν_{xy} and ν_{yx}); Debye temperature of largest phonon frequency (θ_D) in K with definition of $\theta_D = h\omega_D/k_B$ related to the maximum acoustic phonon frequency; 2D thermal conductivity along both directions in nW K^{-1} at room temperature. The mechanical and thermal values of phosphorene[6–9] and SnSe[10] are collected from known literatures. For tellurene, values of mechanical properties are calculated from the elastic solid theory.[11] We can find the sound velocities of tellurene are smaller than 2D SnSe and phosphorene. Moreover, tellurene has the smallest E, G, and ν along both directions in thee of them, indicating a lower vibrational strength.

	υ^x_{TA}	υ^y_{TA}	υ^x_{LA}	υ^y_{LA}	E_x	E_y	G	ν_{xy}	ν_{yx}	θ_D	κ_x	κ_y	κ_y/κ_x
Phosphorene	7.20	6.78	9.78	7.29	44.0	166.0	41.0	0.17	0.62	286	17.69	81.85	4.63
2D SnSe	2.30	2.18	2.97	3.13	23.72	45.14	30.12	0.41	0.81	87	1.52	1.74	1.14
Tellurene	**1.53**	**1.55**	**2.43**	**2.19**	**19.47**	**35.18**	**11.52**	**0.26**	**0.48**	**106**	**1.33**	**2.51**	**1.89**

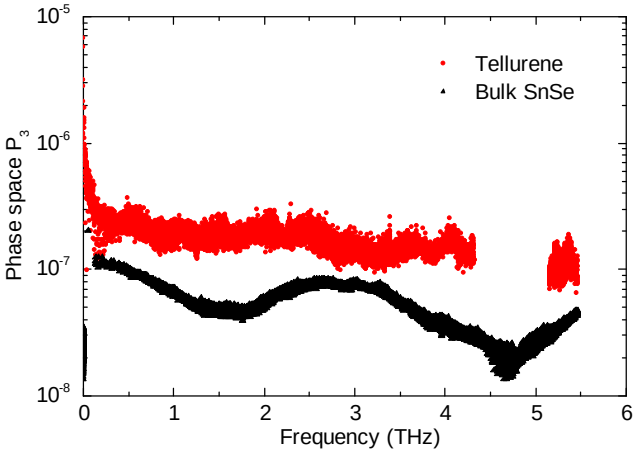

Fig. S3: Phase-space volumes P_3 for three-phonon scattering processes of tellurene and bulk SnSe that is an outstanding thermoelectric materials due to its ultralow κ_L. The inverse of P_3 is proportional to the phonon relaxation time and thus κ_L.

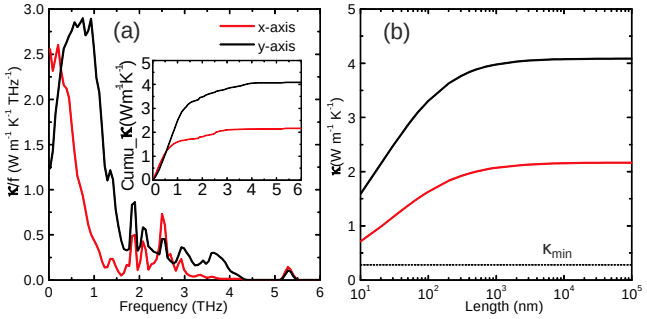

Fig. S4: (a) Frequency-resolved thermal conductivity for tellurene in x and y directions at room temperature. The inset shows the corresponding cumulative thermal conductivity as a function of phonon frequency. (b) The room-temperature thermal conductivity of tellurene as a function sample size along x and y directions. The dashed line is the lower limit κ_{min} of bulk Te according to the Cahill model.[1,3]

and y directions shown in Fig. S4a. As we discussed above, there is a strong coupling between a-o phonon modes in tellurene, therefore the contribution of the acoustic phonon modes to the total κ_L will be weaken. 90% of the κ_L contribution originates from the frequency lower than 2.50 THz for thermal transport in both directions shown in the inset of Fig. S4a.

In practical experiment and device application, boundary (BDR) scattering must be considered. Usually, in nanostructures, κ_L is reduced by BDR scattering that can be evaluated as[14–16]

$$\frac{1}{\tau_\lambda^B} = \frac{\upsilon_\lambda}{L}, \tag{2}$$

where *L* is the size of material. Fig. S4b shows the κ_L of tellurene as a function of *L*. As we can see, κ_L is strongly dependent on the sample size. BDR scattering effect is more distinct when the material become smaller and smaller. For a characteristic size of 50 nm, κ_L along x and y directions are 1.37 and 2.86 W m^{-1} K^{-1}, with a reduction of 36.6% and 29.9% compared with the infinitely large system. For comparison, We also plot the κ_L as a function of temperature considering BDR scattering in Fig. S1 as reference. Hence including the BDR scattering provides an avenue to further decrease the κ_L of tellurene.

VI. Discussion about Slack model in 2D materials

In general, the κ_L of a crystal at finite temperature T can be written as

$$\kappa_L = \frac{1}{3}\int_0^{\omega_{max}} C_s(\omega)\upsilon_g^2(\omega)\tau(\omega)d\omega \tag{3}$$

where υ_g is the group velocity, τ is the relaxation time and C_s is the specific heat of phonon modes.

The fundamental difference between 3D and 2D is the acoustic phonon modes. In 3D materials, there are three linear acoustic phonon modes, whereas in 2D, there are only two linear (LA and TA) and one quadratic ZA acoustic phonon mode whose vibration direction is in the out-of plane. Both frequencies of linear and quadratic acoustic phonon modes are listed as follows:

$$\omega = cq \tag{4}$$

$$\omega = c'q^2 \tag{5}$$

From the group velocity of phonon mode, defined as $\upsilon = \frac{d\omega}{dq}$, we can obtain:

$$\upsilon_g = c \tag{6}$$

$$\upsilon_g = 2c'q \tag{7}$$

for linear and quadratic ZA acoustic phonon modes. Then based on the definition of specific heat:

$$C_\upsilon = \hbar\omega\int_0^{\omega_{max}} g(\omega)\frac{\partial f}{\partial T}d\omega \tag{8}$$

we can get the DOS for linear acoustic and quadratic acoustic ZA mode:

$$g(\omega) = \frac{V}{(2\pi)^3}\int\frac{ds}{|\nabla_q\omega|} \propto (\omega_D^a)^2 \tag{9}$$

$$g(\omega) = \frac{V}{(2\pi)^3}\int\frac{dl}{|\nabla_q\omega|} = const \tag{10}$$

where ω_D^a is the largest acoustic phonon frequency. One can easily get that the integration of the DOS of the linear mode over frequency contributes to a third power relationship of κ_L to frequency ω_D^a, whereas, of the quadratic mode contributes to a first power relationship.

References

(1) Lin, S.; Li, W.; Chen, Z.; Shen, J.; Ge, B.; Pei, Y. Tellurium as a high-performance elemental thermoelectric. *Nat. Commnun.* **2016**, *7*, 10287.

(2) Peng, H.; Kioussis, N.; Stewart, D. A. Anisotropic lattice thermal conductivity in chiral tellurium from first principles. *Appl. Phys. Lett.* **2015**, *107*, 251904.

(3) Cahill, D. G.; Watson, S. K.; Pohl, R. O. Lower limit to the thermal conductivity of disor-

Table S2: Collected relevant physical properties from all available published papers with utmost endeavor in 2D materials. ω_D^a and ω_Γ^o are the largest acoustic phonon frequency and the lowest optical phonon frequency at Γ point in THz. Here, effective vdW thickness d in Å is defined as the summation of the buckling distance and two vdW radii of the outmost surface atoms of structures.[11] Intrinsic κ_{3D} and κ_{2D} are the room temperature 3D thermal conductivity in W $m^{-1}K^{-1}$ and 2D thermal conductivity in 10^{-10} W K^{-1}. All intrinsic κ_L are the smaller one if the material is anisotropic along x and y directions.

2D materials	ω_D^a	ω_Γ^o	κ_{3D}	d	κ_{2D}
Graphene[17]	41.0	27.0	3600	3.35	12060
BN[18,19]	37.5	26.7	1055	3.33	3513.15
MoS_2[20]	6.90	8.25	103.3	6.15	635.30
$MoSe_2$[20,21]	4.71	5.19	54.3	6.47	351.32
$MoTe_2$[22]	4.74	5.10	42.2	7.73	326.21
WS_2[20]	5.40	8.55	141.8	6.16	873.49
WSe_2[20,23]	4.18	5.32	52.6	6.48	340.85
WTe_2[24]	2.55	2.39	9	7.009	63.08
ZrS_2[20]	5.40	5.70	13.3	5.85	77.81
HfS_2[20]	4.32	5.55	16.5	5.88	97.02
$ZrSe_2$[20,25]	3.8	2.40	10.1	6.15	62.12
$HfSe_2$[20]	3.8	2.20	11.3	6.14	69.38
InSe[26]	2.15	1.15	27.6	8.32	229.63
Nitrogene[27]	20.1	28.8	763.4	3.80	2900.92
Silicene[28]	5.6	5.6	19.34	4.2	81.228
Germanene[28]	2.9	4.9	10.52	4.22	44.39
Stanane[28,29]	1.50	3.60	11.6	4.34	50.34
Antimonene[30]	2.10	4.80	15.1	5.77	87.13
Arsenene[27]	3.75	6.60	37.8	5.1	192.78
Phosphorene[31]	6.24	3.93	5.46	5.36	29.27
Blue Phosphorous[32]	7.1	13	78	4.84	377.52
Graphane[18,33]	24.4	33.75	1834	3.60	6600
Fluorographene[18,33]	9.60	7.50	250.4	3.28	821.1
Penta-Graphene[34,35]	14.8	17.5	645	4.6	2967
GeS[36]	2.04	2.52	2.94	5.36	15.76
GeSe[36]	2.55	2.10	4.57	5.56	25.41
SnS[36]	1.81	1.50	2.95	5.71	16.86
SnSe[36]	1.81	1.29	2.59	5.89	15.25
GaN[37]	11.4	21.45	14.93	3.74	55.84
Bismuth[38]	1.35	3.2	16.02	5.87	94.04
Tellurene (this work)	**2.21**	**0.54**	**2.16**	**6.16**	**13.31**

dered crystals. *Phys. Rev. B: Condens. Matter Mater. Phys.* **1992**, *46*, 6131.

(4) Liu, D.; Every, A. G.; Tománek, D. Continuum approach for long-wavelength acoustic phonons in quasi-two-dimensional structures. *Phys. Rev. B: Condens. Matter Mater. Phys.* **2016**, *94*, 165432.

(5) Carrete, J.; Li, W.; Lindsay, L.; Broido, D. A.; Gallego, L. J.; Mingo, N. Physically founded phonon dispersions of few-layer materials and the case of borophene. *Mater. Res. Lett.* **2016**, *4*, 204–211.

(6) Jiang, J.-W. Thermal conduction in single-layer black phosphorus: highly anisotropic? *Nanotech.* **2015**, *26*, 055701.

(7) Wei, Q.; Peng, X. Superior mechanical flexibility of phosphorene and few-layer black phosphorus. *Appl. Phys. Lett.* **2014**, *104*, 251915.

(8) Jain, A.; McGaughey, A. J. Strongly anisotropic in-plane thermal transport in single-layer black phosphorene. *Sci. Rep.* **2015**, *5*, 8501.

(9) Xu, W.; Zhu, L.; Cai, Y.; Zhang, G.; Li, B. Direction dependent thermal conductivity of monolayer phosphorene: Parameterization of Stillinger-Weber potential and molecular dynamics study. *J. Appl. Phys.* **2015**, *117*, 214308.

(10) Qin, G.; Qin, Z.; Fang, W.-Z.; Zhang, L.-C.; Yue, S.-Y.; Yan, Q.-B.; Hu, M.; Su, G. Diverse anisotropy of phonon transport in two-dimensional group IV–VI compounds: A comparative study. *Nanoscale* **2016**, *8*, 11306–11319.

(11) Gao, Z.; Dong, X.; Li, N.; Ren, J. Novel Two-Dimensional Silicon Dioxide with in-Plane Negative Poisson's Ratio. *Nano Lett.* **2017**, *17*, 772–777.

(12) Lindsay, L.; Broido, D. Three-phonon phase space and lattice thermal conductivity in semiconductors. *Journal of Physics: Condensed Matter* **2008**, *20*, 165209.

(13) Li, W.; Carrete, J.; Katcho, N. A.; Mingo, N. ShengBTE: a solver of the Boltzmann transport equation for phonons. *Comput. Phys. Commun.* **2014**, *185*, 1747.

(14) Balandin, A. A. Thermal properties of graphene and nanostructured carbon materials. *Nat. Mater.* **2011**, *10*, 569–581.

(15) Nika, D. L.; Pokatilov, E. P.; Askerov, A. S.; Balandin, A. A. Phonon thermal conduction in graphene: Role of Umklapp and edge roughness scattering. *Phys. Rev. B: Condens. Matter Mater. Phys.* **2009**, *79*, 155413.

(16) Zhu, L.; Zhang, G.; Li, B. Coexistence of size-dependent and size-independent thermal conductivities in phosphorene. *Phys. Rev. B: Condens. Matter Mater. Phys.* **2014**, *90*, 214302.

(17) Lindsay, L.; Li, W.; Carrete, J.; Mingo, N.; Broido, D. A.; Reinecke, T. L. Phonon thermal transport in strained and unstrained graphene from first principles. *Phys. Rev. B: Condens. Matter Mater. Phys.* **2014**, *89*, 155426.

(18) Cepellotti, A.; Fugallo, G.; Paulatto, L.; Lazzeri, M.; Mauri, F.; Marzari, N. Phonon hydrodynamics in two-dimensional materials. *Nat. Commun.* **2015**, *6*, 6400.

(19) Michel, K.; Verberck, B. Theoretical phonon dispersions in monolayers and multilayers of hexagonal boron-nitride. *Phys. Status Solidi b* **2009**, *246*, 2802–2805.

(20) Gu, X.; Yang, R. Phonon transport in single-layer transition metal dichalcogenides: A first-principles study. *Appl. Phys. Lett.* **2014**, *105*, 131903.

(21) Horzum, S.; Sahin, H.; Cahangirov, S.; Cudazzo, P.; Rubio, A.; Serin, T.; Peeters, F. M. Phonon softening and direct to indirect band gap crossover in strained single-layer $MoSe_2$. *Phys. Rev. B: Condens. Matter Mater. Phys.* **2013**, *87*, 125415.

(22) Shafique, A.; Shin, Y.-H. Strain engineering of phonon thermal transport properties in monolayer 2H-$MoTe_2$. *Phys. Chem. Chem. Phys.* **2017**, *19*, 32072–32078.

(23) Huang, W.; Luo, X.; Gan, C. K.; Quek, S. Y.; Liang, G. Theoretical study of thermoelectric properties of few-layer MoS_2 and WSe_2. *Phys. Chem. Chem. Phys.* **2014**, *16*, 10866–10874.

(24) Ma, J.; Chen, Y.; Han, Z.; Li, W. Strong anisotropic thermal conductivity of monolayer WTe_2. *2D Mater.* **2016**, *3*, 045010.

(25) Ding, G.; Gao, G.; Huang, Z.; Zhang, W.; Yao, K. Thermoelectric properties of monolayer MSe2 (M= Zr, Hf): low lattice thermal conductivity and a promising figure of merit. *Nanotechnology* **2016**, *27*, 375703.

(26) Nissimagoudar, A. S.; Ma, J.; Chen, Y.; Li, W. Thermal transport in monolayer InSe. *J. Phys.: Condens. Matter* **2017**, *29*, 335702.

(27) Peng, B.; Zhang, D.; Zhang, H.; Shao, H.; Ni, G.; Zhu, Y.; Zhu, H. The conflicting role of buckled structure in phonon transport of 2D group-IV and group-V materials. *Nanoscale* **2017**, *9*, 7397–7407.

(28) Kuang, Y.; Lindsay, L.; Shi, S.; Zheng, G. Tensile strains give rise to strong size effects for thermal conductivities of silicene, germanene and stanene. *Nanoscale* **2016**, *8*, 3760–3767.

(29) Peng, B.; Zhang, H.; Shao, H.; Xu, Y.; Zhang, X.; Zhu, H. Low lattice thermal conductivity of stanene. *Sci. Rep.* **2016**, *6*, 20225.

(30) Wang, S.; Wang, W.; Zhao, G. Thermal transport properties of antimonene: an ab initio study. *Phys. Chem. Chem. Phys.* **2016**, *18*, 31217–31222.

(31) Qin, G.; Zhang, X.; Yue, S.-Y.; Qin, Z.; Wang, H.; Han, Y.; Hu, M. Resonant bonding driven giant phonon anharmonicity and low thermal conductivity of phosphorene. *Phys. Rev. B: Condens. Matter Mater. Phys.* **2016**, *94*, 165445.

(32) Jain, A.; McGaughey, A. J. Strongly anisotropic in-plane thermal transport in single-layer black phosphorene. *Sci. Rep.* **2015**, *5*.

(33) Peelaers, H.; Hernandez-Nieves, A.; Leenaerts, O.; Partoens, B.; Peeters, F. Vibrational properties of graphene fluoride and graphane. *Appl. Phys. Lett.* **2011**, *98*, 051914.

(34) Zhang, S.; Zhou, J.; Wang, Q.; Chen, X.; Kawazoe, Y.; Jena, P. Penta-graphene: A new carbon allotrope. *Proc. Natl. Acad. Sci. U. S. A.* **2015**, *112*, 2372–2377.

(35) Wang, F. Q.; Yu, J.; Wang, Q.; Kawazoe, Y.; Jena, P. Lattice thermal conductivity of penta-graphene. *Carbon* **2016**, *105*, 424–429.

(36) Qin, G.; Qin, Z.; Fang, W.-Z.; Zhang, L.-C.; Yue, S.-Y.; Yan, Q.-B.; Hu, M.; Su, G. Diverse anisotropy of phonon transport in two-dimensional group IV–VI compounds: A comparative study. *Nanoscale* **2016**, *8*, 11306–11319.

(37) Qin, Z.; Qin, G.; Zuo, X.; Xiong, Z.; Hu, M. Orbitally driven low thermal conductivity of monolayer gallium nitride (GaN) with planar honeycomb structure: a comparative study. *Nanoscale* **2017**, *9*, 4295–4309.

(38) Zhang, D.-C.; Zhang, A.-X.; Guo, S.-D.; Duan, Y.-f. Thermoelectric properties of β-As, Sb and Bi monolayers. *RSC Adv.* **2017**, *7*, 24537–24546.